Hindawi
International Journal of Antennas and Propagation
Volume 2019, Article ID 9582564, 13 pages
https://doi.org/10.1155/2019/9582564

Research Article

Design of Multilayer Frequency-Selective Surfaces by Equivalent Circuit Method and Basic Building Blocks

Yuan Xu and Mang He

School of Information and Electronics, Beijing Institute of Technology, Beijing 100081, China

Correspondence should be addressed to Mang He; hemang@bit.edu.cn

Received 20 March 2019; Accepted 27 June 2019; Published 14 August 2019

Academic Editor: María Elena de Cos Gómez

An equivalent circuit method (ECM) is proposed for the design of multilayer frequency-selective surfaces (FSSs). In contrast to the existing ECMs that were developed mainly for the analysis of the properties of a given FSS, the presented ECM aims at providing the initial design parameters of an FSS from the desired frequency response. In this method, four types of basic FSS structures are used as the building blocks to construct the multilayer FSSs, and their surface impedances in both the normal- and the oblique-incidence situations are studied in detail in order to achieve more accurate equivalent circuit (EC) representation of the entire FSS. For a general FSS design with expected frequency response, the EC parameters and the geometrical sizes of the required basic building blocks can be synthesized from a few typical S-parameter (S_{11}/S_{12}) samplings of the response curves via a simple least-square curve-fitting process. The effectiveness and accuracy of the method are shown by the designs of a band-pass FSS with steep falling edge and a miniaturized band-pass FSS with out-of-band absorption. The prototype of one design is fabricated, and the measured frequency response agrees well with the numerical results of the ECM and the full-wave simulations.

1. Introduction

As a kind of periodic structures, frequency-selective surfaces (FSSs) are widely used as spatial-frequency filters in many applications, such as hybrid radomes, absorbing materials, and electromagnetic shielding devices [1, 2]. It is important to find efficient and fast methods to expedite the design of FSSs with specified requirements. In the existing literature, the design of FSS mainly relies on the full-wave numerical software, and parametric sweep is an indispensable process. However, although the numerical simulations yield accurate frequency response for a given FSS structure, they cannot provide adequate information on how to start an FSS design and how to initialize the geometrical sizes of the design to fulfill the expected frequency response of a general form. As a powerful analysis tool, the equivalent circuit method (ECM) is often utilized to reveal the operation principles of an FSS and to provide an approximate frequency response with acceptable accuracy to the designers [3–5], but we can rarely find the FSS designs that are implemented by using the ECM as a design tool according to the required frequency response [6].

In general, in order to realize a filter with an arbitrary desired frequency response, one usually needs four types of basic circuits that can provide the high-pass (HP), low-pass (LP), band-pass (BP), and band-stop (BS) filtering functionalities. Among many FSS designs [3–9], the FSSs consisting of the strip grid (SG), the square patch (SP), the square slot (SS), and the square loop (SL) elements present excellent HP, LP, BP, and BS performances, respectively, in terms of insensitivity to the polarization and angle of incidence. Therefore, in principle, these four types of basic structures are good candidates which can be used to construct FSSs with more complicated and required properties.

In this paper, based on the ECM and using the abovementioned four types of basic FSSs as the building blocks, we try to present a fast and simple design method for the multilayer FSS with desired frequency response. To achieve this goal, the EC representations of the basic

structures, which are functions of the angle of incidence, polarization, geometrical dimensions, and material properties, should be derived with adequate accuracy first. The surface impedances of the SG and SP were well studied in [10–12], and the formulations that relate the equivalent inductance L and capacitance C with the geometrical parameters of the SG and SP at normal incidence are given in [7]. However, these works did not consider the effects of the dielectric substrate in the oblique-incidence case. In [13], more accurate derivations for the surface impedances of the SG and SP were proposed for oblique incidence. The surface impedance of other two basic structures, i.e., SS and SL, has been investigated in [14–17]. Based on these studies, one of the objectives of this paper is to derive the EC parameters of the four types of basic structures for both normal and oblique incidence and then to complete the EC representations of the four building blocks. Subsequently, the transmission matrix of the multilayer FSS at arbitrary angle of incidence can be obtained by using the transmission line models for the dielectric substrates [7, 8] and the ECs of the basic building blocks. Through the transmission matrix whose entry is explicit analytical function of the physical sizes of the basic FSSs, the geometrical parameters of the multilayer FSS can be achieved from the samplings of the desired frequency response for different angles and polarizations of incidence by using the least-square curve-fitting method.

In the remainder of the paper, the surface impedances of the four basic structures, as well as the transmission matrix of the multilayer FSS, are derived in the second section. Then, the design procedure is exemplified by two examples, and the effectiveness and accuracy of the proposed method are verified by the full-wave simulations. After that, we present the results of measurement and give the conclusions in the last section.

2. EC Representations of the Multilayer FSS

2.1. Surface Impedance of the Four Types of Basic FSSs. As stated above, in order to get the EC representation of the entire multilayer FSS, we should first derive the formulations of surface impedances for the four basic building blocks at each layer. The structures of the basic FSSs, the SG, the SP, the SS, and the SL, are shown in Figure 1. In general case, these metallic arrays may locate in a homogeneous media or at the interface of two different dielectric substrates. In reference [13], the surface impedances of the SG (Figure 1(a)) and SP (Figure 1(b)) were studied in detail, which are inductive and capacitive, respectively. Based on [13], the characteristics of the latter two basic FSS structures, SS (Figure 1(d)) and SL (Figure 1(c)), are derived here. To derive complete analytical formulations of the surface impedances, we classified the four basic FSSs into two categories: the first one is called the *grid-type* structure, which includes the SG and SS, while the second one is named the *patch-type* structure that includes the SP and SL. As seen in Figure 1(a), the two-dimensional metallic SG resides in the xoy plane with the periodicity being D in both x- and y-directions. When the width of the grid w is much smaller than D ($w << D$), the averaged tangential component of the total electric field E_ν^{tot} can be related with the averaged surface current density J_ν along the ν-axis ($\nu = x$ or y) by the surface impedance Z_g^κ ($\kappa =$ TE or TM) of the SG as $E_\nu^{\text{tot}} = Z_g^\kappa J_\nu$ [13]. Therefore, if the yoz plane is the plane of incidence, then the relationships become $E_x^{\text{tot}} = Z_g^{\text{TE}} J_x$ and $E_y^{\text{tot}} = Z_g^{\text{TM}} J_y$ for the TE and TM polarizations, respectively. For arbitrary angle of incidence, the surface impedance of the SG under the TE- and TM-polarized plane wave is

$$Z_g^{\text{TE}} = j\frac{\eta_{\text{eff}}}{2}\alpha, \tag{1}$$

$$Z_g^{\text{TM}} = j\frac{\eta_{\text{eff}}}{2}\alpha\xi, \tag{2}$$

respectively. $\eta_{\text{eff}} = \sqrt{\mu_0\mu_{\text{eff}}/(\varepsilon_0\varepsilon_{\text{eff}})}$ is the intrinsic impedance of the effective dielectric substrate in which the SG resides. If the SG locates in a single substrate with electromagnetic (EM) parameters μ_{r} and ε_{r}, then $\mu_{\text{eff}} = \mu_{\text{r}}$ and $\varepsilon_{\text{eff}} = \varepsilon_{\text{r}}$; if the SG is at the interface of two substrates with different EM parameters (ε_{r1}, μ_{r1}) and (ε_{r2}, μ_{r2}), then the relative effective permittivity and permeability can be averaged as $\varepsilon_{\text{eff}} = (\varepsilon_{\text{r1}} + \varepsilon_{\text{r2}})/2$ and $\mu_{\text{eff}} = (\mu_{\text{r1}} + \mu_{\text{r2}})/2$. α is defined as the grid parameter in [10] for an electrically dense array of SG (i.e., $w << D$, $k_{\text{eff}}D << 2\pi$):

$$\alpha = \frac{k_{\text{eff}}D}{\pi}\ln\left(\frac{1}{\sin(\pi w/2D)}\right), \tag{3}$$

where $k_{\text{eff}} = k_0\sqrt{\varepsilon_{\text{eff}}}$ is the effective wave number and μ_0, ε_0, and k_0 are the permeability, permittivity, and wave number in free space, respectively. In equation (2), the SG's surface impedance for the TM polarization is a function of the angle of incidence θ, and the dependence is included in ξ as $\xi = (1 - k_0^2\sin^2\theta)/2k_{\text{eff}}^2$ [13].

Since the SP is a complementary structure of the SG, its surface impedance Z_p^κ can be easily obtained by applying Babinet's principle:

$$Z_g^{\text{TE}} Z_p^{\text{TM}} = \frac{\eta_{\text{eff}}^2}{4}, \qquad Z_p^{\text{TE}} Z_g^{\text{TM}} = \frac{\eta_{\text{eff}}^2}{4}. \tag{4}$$

Thus, Z_p^{TE} and Z_p^{TM} read

$$Z_p^{\text{TE}} = -j\frac{\eta_{\text{eff}}}{2\alpha\xi}, \tag{5}$$

$$Z_p^{\text{TM}} = -j\frac{\eta_{\text{eff}}}{2\alpha}. \tag{6}$$

In equations (1) and (6), we note that the surface impedances Z_g^{TE} and Z_p^{TM} do not change when θ varies. In addition, we find that the SG and SP act as an inductor and a capacitor, respectively. At normal incidence, in one periodicity, the equivalent inductance L for the SG and the equivalent capacitance C for the SP can be calculated by equations (1) and (6) as

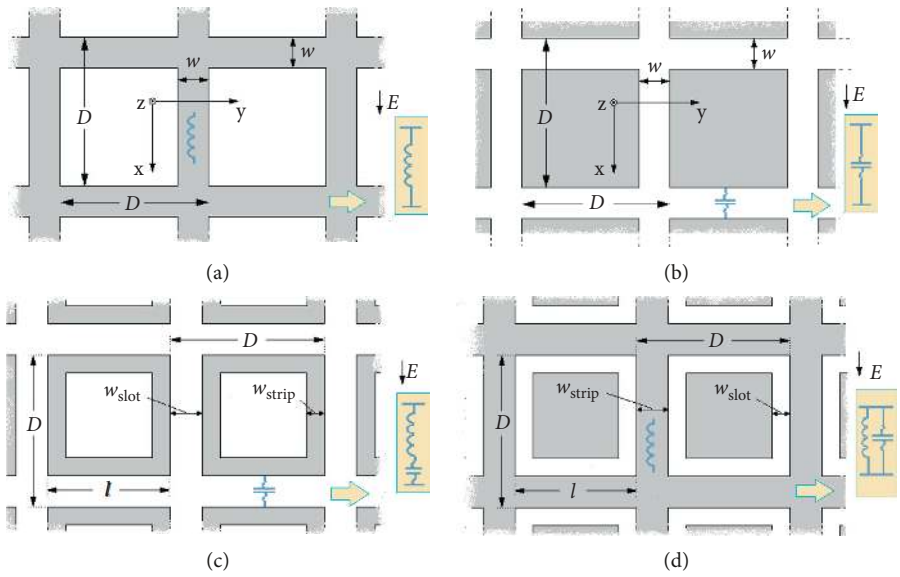

Figure 1: The four FSS structures as the building blocks of multilayer FSSs. (a) Square grids (SGs). (b) Square patches (SPs). (c) Square loops (SLs). (d) Square slots (SSs). Metallic parts are colored in grey.

$$L_g = \frac{\eta_{\text{eff}}}{2\omega}\alpha, \tag{7}$$

$$C_p = \frac{2\alpha}{\eta_{\text{eff}}\omega}, \tag{8}$$

respectively. Then, the per-unit-length inductance of the strip in the SG structure is

$$L_i = \frac{L_g}{D} = \mu_0\mu_{\text{eff}}\frac{1}{2\pi}\ln\left(\frac{1}{\sin\left(\pi w_{\text{strip}}/2D\right)}\right), \tag{9}$$

and the per-unit-length capacitance of the slot between two adjacent patches in the SP structure is

$$C_i = \frac{C_p}{D} = \varepsilon_0\varepsilon_{\text{eff}}\frac{2}{\pi}\ln\left(\frac{1}{\sin\left(\pi w_{\text{slot}}/2D\right)}\right), \tag{10}$$

where w_{strip} is the width of the strip and w_{slot} is the width of the slot as shown in Figures 1(c) and 1(d), respectively.

The SS shown in Figure 1(d) is classified as the *grid-type* FSS element, since it can be seen as a modified version of the SG by inserting a metallic square patch into the metallic grid. Thus, its equivalent surface impedance under arbitrary angle of incidence can also be written in the same form as the SG, like equations (1) and (2):

$$\begin{aligned} Z^{\text{TE}}_{\text{grid-type}} &= Z^{\perp}_{\text{grid-type}}, \\ Z^{\text{TM}}_{\text{grid-type}} &= Z^{\perp}_{\text{grid-type}}\xi, \end{aligned} \tag{11}$$

where $Z^{\perp}_{\text{grid-type}}$ is the surface impedance of the *grid-type* FSS element at normal incidence. It should be noted that the inserted patch will introduce two additional capacitances because two slots with the length of l are formed between the metallic grid and the inserted patch. The two serial capacitances are then in parallel connection with the inductance of the SG, which means that the SS can be seen as a parallel LC resonant circuit from the EC point of view. The EC of the SS is shown in the inset of Figure 1(d). Thus, the SS's surface impedance can be computed as

$$Z^{\text{TE}}_{\text{ss}} = j\omega L_{\text{ss}} \left\| \frac{1}{j\omega C_{\text{ss}}}, \right. \tag{12}$$

$$Z^{\text{TM}}_{\text{ss}} = \left(j\omega L_{\text{ss}} \left\| \frac{1}{j\omega C_{\text{ss}}} \right. \right)\xi, \tag{13}$$

where the symbol "||" means parallel connection. In equations (12) and (13), the inductance L_{ss} and capacitance C_{ss} are obtained from the per-unit-length inductance and the per-unit-length capacitance defined in equations (9) and (10), respectively,

$$\begin{aligned} L_{\text{ss}} &= lL_i, \\ C_{\text{ss}} &= \frac{(l - 2w_{\text{slot}})C_i}{2}. \end{aligned} \tag{14}$$

Similarly, the SL in Figure 1(c) is categorized as the *patch-type* FSS element, since the square loop can be seen as a variation of the SP by removing the central part of the metallic patch. So, its equivalent surface impedance under the plane wave incidence of arbitrary angle can also be written in the same form as the SP, like equations (5) and (6):

$$\begin{aligned} Z^{\text{TE}}_{\text{patch-type}} &= \frac{Z^{\perp}_{\text{patch-type}}}{\xi}, \\ Z^{\text{TM}}_{\text{patch-type}} &= Z^{\perp}_{\text{patch-type}}, \end{aligned} \tag{15}$$

where $Z^{\perp}_{\text{patch-type}}$ is the surface impedance of the *patch-type* FSS element at normal incidence. It is noted that an additional inductance is formed since the original square metallic patch is changed into a square loop due to the removal of its central part. This inductance is in serial

connection with the capacitance of the SP, which indicates that the SL can be seen as a serial LC resonant circuit from the EC point of view. The EC of the SL is shown in the inset of Figure 1(c). Thus, the surface impedance of SL can be computed as

$$Z_{\mathrm{sl}}^{\mathrm{TE}} = \frac{\left(j\omega L_{\mathrm{sl}} + \left(1/j\omega C_{\mathrm{sl}}\right)\right)}{\xi}, \tag{16}$$

$$Z_{\mathrm{sl}}^{\mathrm{TM}} = j\omega L_{\mathrm{sl}} + \frac{1}{j\omega C_{\mathrm{sl}}}. \tag{17}$$

In equations (16) and (17), if the side length of the square loop is l, the inductance L_{sl} and capacitance C_{sl} can also be obtained from the per-unit-length inductance and capacitance, respectively,

$$\begin{aligned} L_{\mathrm{sl}} &= lL_i, \\ C_{\mathrm{sl}} &= lC_i. \end{aligned} \tag{18}$$

By now, the equivalent surface impedances of the four basic building blocks have been derived completely for arbitrary angle of incidence, which closely relate the EC representations of the basic FSS structures to their physical dimensions.

2.2. Transmission Matrix of the Multilayer FSS. For a multilayer FSS composed of n-layer FSSs and $(n-1)$-layer dielectric substrates as shown in Figure 2, the transmission matrix can be constructed using the transmission line model. The ABCD matrix for a single dielectric layer is written as [8]

$$\begin{bmatrix} A & B \\ C & D \end{bmatrix} = \begin{bmatrix} \cosh(j\nu d) & Z_c^{\mathrm{TE,TM}} \sinh(j\nu d) \\ \dfrac{\sinh(j\nu d)}{Z_c^{\mathrm{TE,TM}}} & \cosh(j\nu d) \end{bmatrix}, \tag{19}$$

where d is the thickness of the dielectric layer, $\nu = k_d \cos\theta'$ is the vertical component of the wave number $k_d = \omega\sqrt{\varepsilon_0 \varepsilon_{\mathrm{r}} \mu_0}$ in the medium, and θ' is the refraction angle when the angle of incidence is θ, which can be calculated from Snell's law:

$$\theta' = \arcsin\left(\frac{\sin\theta}{\sqrt{\varepsilon_{\mathrm{r}}}}\right). \tag{20}$$

In equation (19), the effects of polarization in the oblique incidence are included in the characteristic impedance $Z_c^{\mathrm{TE,TM}}$ as

$$\begin{aligned} Z_c^{\mathrm{TE}} &= \frac{\left(\eta_0/\sqrt{\varepsilon_r}\right)}{\cos\theta'}, \\ Z_c^{\mathrm{TM}} &= \frac{\eta_0}{\sqrt{\varepsilon_r}} \cos\theta', \end{aligned} \tag{21}$$

where η_0 is the intrinsic wave impedance in free space. Then, the transmission matrix of the entire multilayer FSS can be obtained by cascading the ABCD matrices for each dielectric layer and the transmission matrices derived from the surface impedances for each layer of the basic FSSs:

$$\begin{aligned} \begin{bmatrix} A & B \\ C & D \end{bmatrix} = {} & \begin{bmatrix} 1 & 0 \\ \dfrac{1}{Z_1^{\mathrm{FSS}}} & 1 \end{bmatrix} \begin{bmatrix} A_1 & B_1 \\ C_1 & D_1 \end{bmatrix} \cdots \begin{bmatrix} 1 & 0 \\ \dfrac{1}{Z_i^{\mathrm{FSS}}} & 1 \end{bmatrix} \begin{bmatrix} A_i & B_i \\ C_i & D_i \end{bmatrix} \cdots \\ & \cdot \begin{bmatrix} 1 & 0 \\ \dfrac{1}{Z_{n-1}^{\mathrm{FSS}}} & 1 \end{bmatrix} \begin{bmatrix} A_{n-1} & B_{n-1} \\ C_{n-1} & D_{n-1} \end{bmatrix} \begin{bmatrix} 1 & 0 \\ \dfrac{1}{Z_n^{\mathrm{FSS}}} & 1 \end{bmatrix}. \end{aligned} \tag{22}$$

The reflection and transmission coefficients of the multilayer FSS are calculated as

$$S_{11} = \frac{\left(A + B/Z_0^{\mathrm{TE,TM}}\right) - \left(Z_0^{\mathrm{TE,TM}} C + D\right)}{\left(A + B/Z_0^{\mathrm{TE,TM}}\right) + \left(Z_0^{\mathrm{TE,TM}} C + D\right)}, \tag{23}$$

$$S_{21} = \frac{2}{\left(A + B/Z_0^{\mathrm{TE,TM}}\right) + \left(Z_0^{\mathrm{TE,TM}} C + D\right)}, \tag{24}$$

where distinct free-space intrinsic wave impedances for TE and TM polarizations are used [8]:

$$\begin{aligned} Z_0^{\mathrm{TE}} &= \frac{\eta_0}{\cos\theta}, \\ Z_0^{\mathrm{TM}} &= \eta_0 \cos\theta. \end{aligned} \tag{25}$$

2.3. Accuracy Validation of the Proposed ECM. In this section, a single-layer FSS composed of SL elements is used to validate the accuracy of the proposed ECM. The configuration of the FSS is shown in Figures 3(a) and 3(b) illustrates the corresponding EC. The geometrical sizes of the FSS are $D = 4.0$ mm, $w_{\mathrm{strip}} = 0.5$ mm, and $l = 3.5$ mm. The thickness of the dielectric substrate is $h = 1.0$ mm, and the relative permittivity and the loss tangent are 2.0 and 0.01, respectively. In Figure 4, the reflection coefficients calculated by the proposed ECM and those simulated by the commercial full-wave software ANSYS HFSS [18] are demonstrated. For the normal incidence, two sets of results are in excellent agreement, while for the 45° oblique incidence, the ECM results deviate slightly from the numerical results at higher frequency, but the largest discrepancy is less than 0.65 dB.

3. Design Procedure of Multilayer FSS by the ECM

It has been shown above that the EC can reproduce the characteristics of the multilayer FSSs constructed by the four basic building blocks with reasonable accuracy. Naturally, we try to use the proposed ECM and the basic FSS structures to design the multilayer FSSs with desired frequency response. To determine the dimensions of the desired FSS structure, the design procedure contains the following:

Step 1: obtain the equivalent circuit model of the FSS

Step 2: derive the impedance of each FSS layer

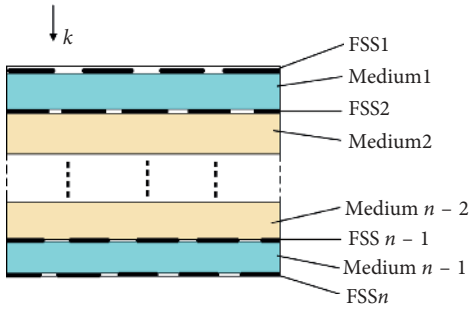

FIGURE 2: Structure of multilayer FSS.

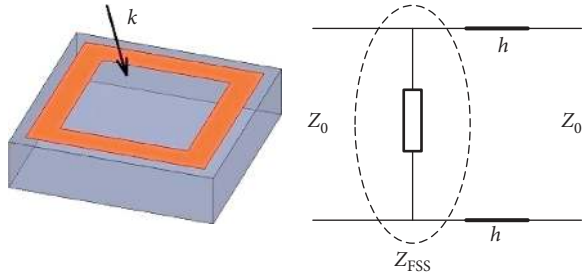

FIGURE 3: Structure of the single-layer band-stop FSS. (a) SL element of the FSS. (b) Equivalent circuit of the FSS.

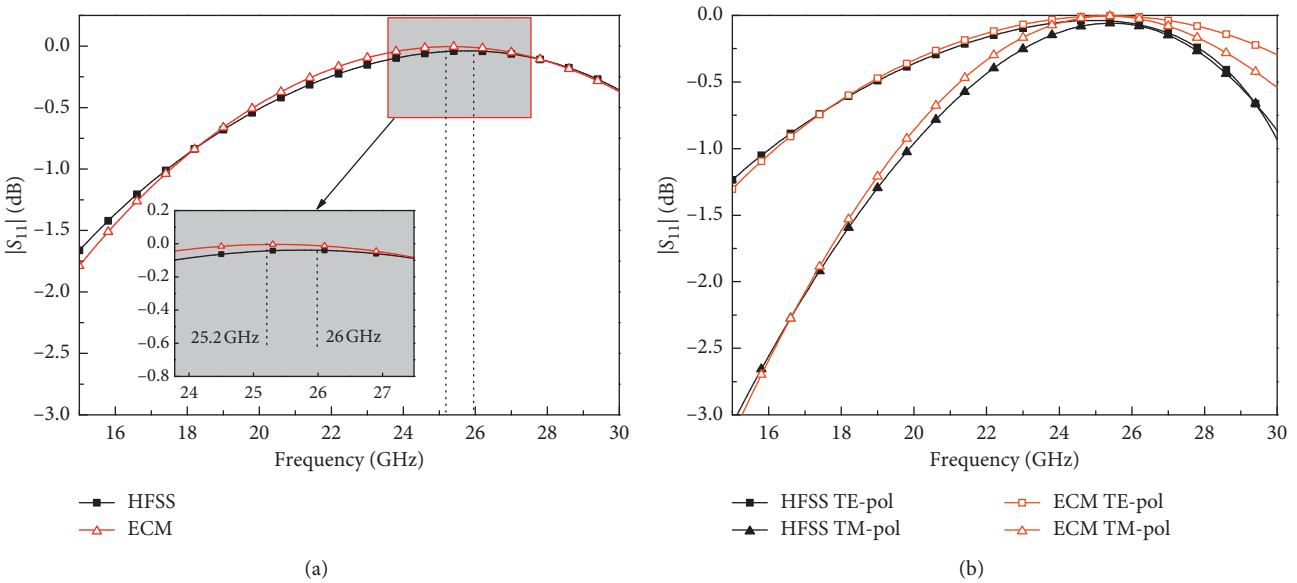

FIGURE 4: Comparison of the reflection coefficients $|S_{11}|$ calculated by the ECM and the numerical results by HFSS. (a) Normal incidence. (b) Oblique incidence with $\theta = 45^\circ$ and different polarizations.

Step 3: build the transmission matrix based on the transmission line principle

Step 4: synthesize the EC parameters and the geometrical sizes of the structure from a few typical S-parameter (S_{11}/S_{21}) samplings of the desired response curves via curve-fitting process to realize the initial dimension estimation of the desired FSS

Step 5: based on the ECM data, sweep the FSS parameters using full-wave simulation software to obtain the optimized parameters and finish the design

In the following, two examples are presented to illustrate the design procedure.

3.1. Design of a Broadband Band-Pass FSS with Fast Falling Edge. The first example is to design a broadband band-pass FSS with a fast falling edge, and the desired transmission coefficient of the FSS is shown in Figure 5. The target FSS should have a passband from 4.5 to 7.0 GHz with ≥70% transmission efficiency (i.e., $|S_{21}| \geq -1.5$ dB) when the angle of incidence is up to 45°, and a stopband from 8 to 11 GHz with $|S_{21}| \leq -20$ dB. Apparently, a very steep falling edge is required from 7.0 to 8.0 GHz.

In general, the FSS composed of the SS elements is a band-pass filter, but it cannot provide fast rising or falling edges. On the other hand, the SG structure has a wideband high-pass response; thus, if it works together with the SL structure that acts as a band-stop filter, then the overall frequency response will consist of a passband and a stopband. To satisfy the steep falling edge requirement, two SL FSS layers with the same element's sizes are used to make $|S_{21}|$ falloff quickly from 7.0 to 8.0 GHz, and the SG FSS layer is sandwiched by the two SL FSSs. The geometry of the final design is shown in Figure 6(a), and Figure 6(b) displays its EC. According to the EC, the surface impedance of the FSS on each layer is

$$Z_1 = Z_3 = Z_{\text{sl}}^{\kappa}, \tag{26}$$

$$Z_2 = Z_g^{\kappa}, \tag{27}$$

where κ is either TE or TM, which is dependent of polarization of incidence. Z_1 and Z_3 follow equations (16) and (17), and Z_2 follows equations (1) and (2). Referring to equations (7)–(10), the circuit parameters L_1, C_1, and L_2 shown in Figure 6(b) are related to the geometrical sizes from equations (26) and (27):

$$L_1 = \mu_0 \frac{l_{\text{loop}}}{2\pi} \ln\left(\frac{1}{\sin\left(\pi w_{\text{loop}}/2D\right)}\right),$$

$$C_1 = \varepsilon_0 \varepsilon_{\text{eff}} \frac{2l_{\text{loop}}}{\pi} \ln\left[\frac{1}{\sin\left(\pi\left(D - l_{\text{loop}}\right)/2D\right)}\right], \tag{28}$$

$$L_2 = \mu_0 \frac{D}{2\pi} \ln\left(\frac{1}{\sin\left(\pi w_{\text{grid}}/2D\right)}\right).$$

Then, from equations (22) and (24), the transmission and reflection coefficients can be expressed as functions of the geometrical parameters of the multilayer FSS and the angle and polarization of incidence. Thus, if the two dielectric substrates are specified in the design, for given polarization and incident angle, then the geometrical parameters l_{loop}, w_{loop}, w_{grid}, and D can be obtained by applying the curve-fitting method [19] on the samplings from the desired S_{11}/S_{21} curve in a least-square sense. The choice of sampling points is quite flexible, and the rule of thumb is that the chosen samplings should manifest the main property of the frequency response. In this design, the samples are extracted from the curve of transmission coefficient as shown in Figure 5, and they distribute evenly in the passband and nonuniformly in other bands. The nine selected sampling frequencies and the corresponding values of $|S_{21}|$ are listed in Table 1.

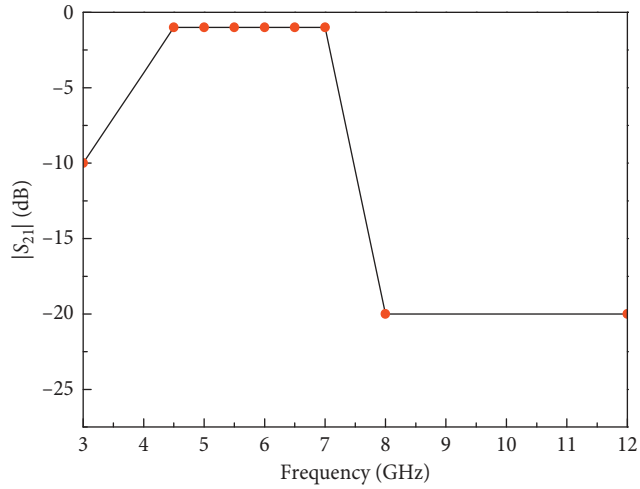

Figure 5: The desired frequency response of the band-pass FSS with steep falling edge. The samplings marked in red color are chosen to show the main properties of the FSS in the passband and stopband.

In this example, the two layers of dielectric substrates are of the same thickness of 1.27 mm and same relative permittivity of 2.2. Two different angles of incidence ($\theta = 0°$ and 45°) and two polarization states (TE and TM) are used to obtain l_{loop}, w_{loop}, w_{grid}, and D, with the desire that the performance of the FSS is stable over a wide range of incident angles under the plane wave illumination with different polarizations. In Table 2, the geometrical sizes under different conditions of incidence are computed and these values are averaged as the final design data of the ECM. Finally, these ECM data are used as the initial values in the parameter-sweep process in the ANSYS HFSS for fine tuning. The optimal values by HFSS are $l_{\text{loop}} = 8.2$ mm, $w_{\text{loop}} = 1.0$ mm, $w_{\text{grid}} = 1.0$ mm, and $D = 10.0$ mm, which are in close proximity to the average sizes given by the proposed ECM.

Figures 7(a) and 7(b) show the computed transmission coefficient of the multilayer FSS with the structure being obtained by the ECM, i.e., the geometrical sizes of the FSS are the average values listed in Table 2. The results of ECM are compared with the numerical ones from HFSS, and the desired response is also plotted as the benchmark. An apparent fast falling edge from 7.0 to 8.0 GHz is observed for different incident polarizations and angles, and the transmission coefficient follows well with the desired response in the passband. In Figure 7(c), after fine tuning of the structure's sizes by the HFSS, simulated $|S_{21}|$ of the FSS with the optimal dimensions are presented, and the transmission efficiency is seen to be improved at oblique incidence. The performance of the FSS is stable over a wide range of the angles of incidence. Meanwhile, it should be noted that the mutual couplings among different FSS layers are not

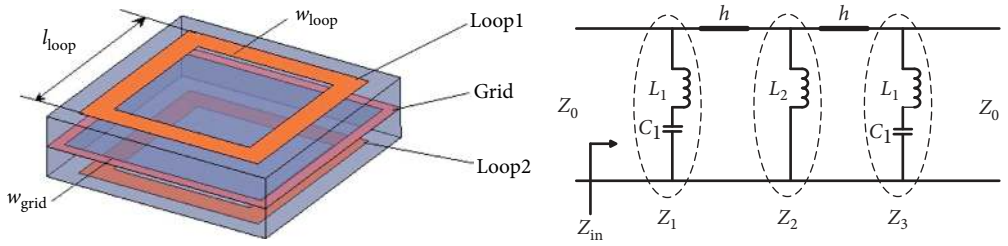

(a) (b)

Figure 6: The configuration and equivalent circuit of the double-layer band-pass FSS with steep falling-edge stopband. (a) Geometry of one element of the FSS. (b) Equivalent circuit.

Table 1: Samples from the desired frequency response of S_{21}.

Sampling frequencies (GHz)	3.0	4.5	5.0	5.5	6.0	6.5	7.0	8.0	12.0
$\|S_{21}\|$ (dB)	−10.0	−1.0	−1.0	−1.0	−1.0	−1.0	−1.0	−20.0	−20.0

Table 2: Geometrical parameters calculated by the curve-fitting method.

θ	l_{loop} (mm)	w_{loop} (mm)	w_{grid} (mm)	D (mm)
0°	8.3	1.0	2.0	10.0
45° TE	8.4	0.9	1.3	10.2
45° TM	8.6	1.6	2.0	9.8
Averaged values	8.4	1.2	1.8	10.0
Optimal values by HFSS parameter sweep	8.2	1.0	1.0	10.0

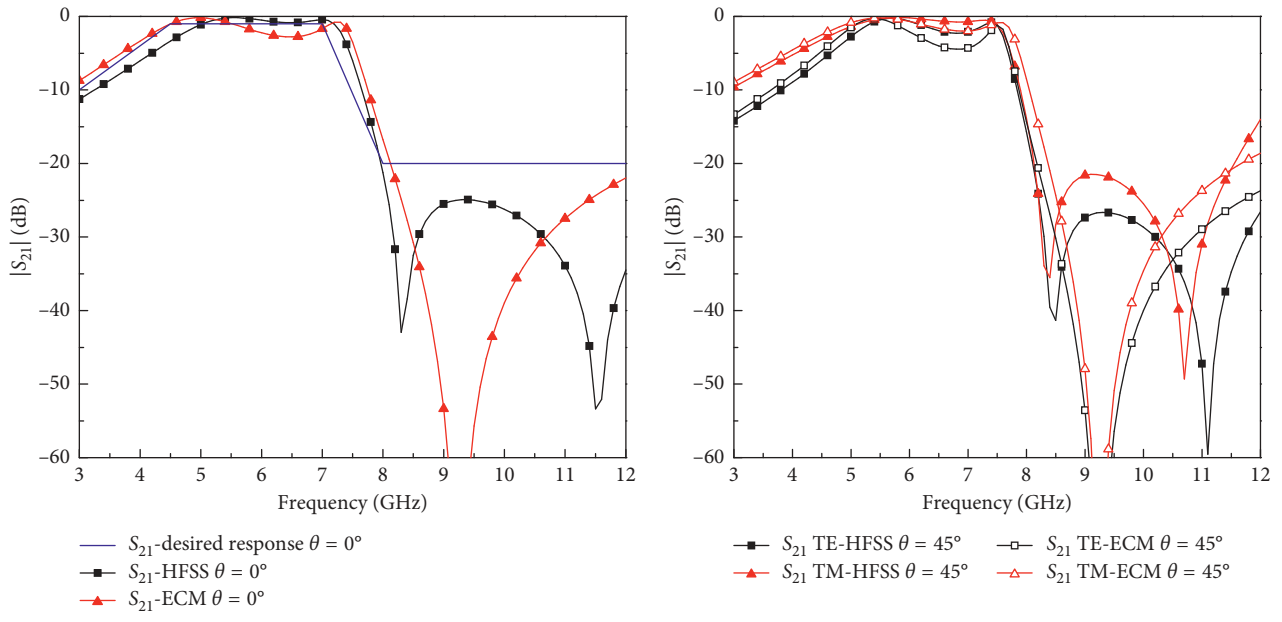

(a) (b)

Figure 7: Continued.

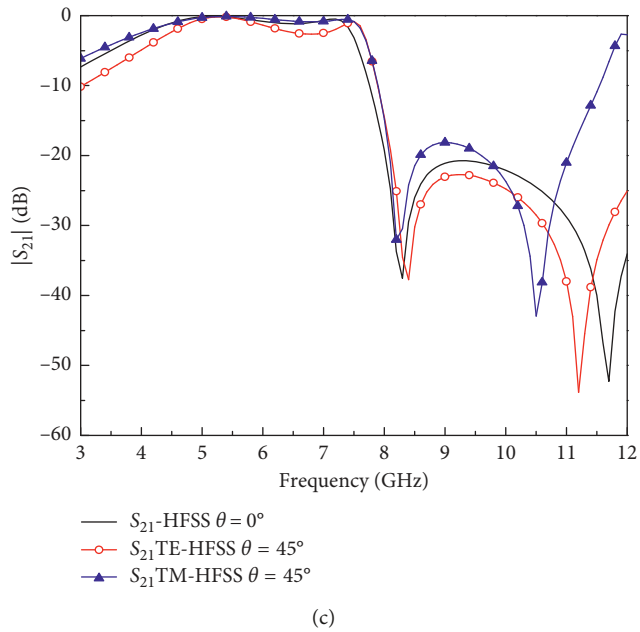

(c)

FIGURE 7: The simulated results using the ECM and HFSS. (a) $|S_{21}|$ of the FSS at normal incidence. (b) $|S_{21}|$ of the FSS at oblique incidence ($\theta = 45^{\circ}$) for TE/TM polarization. (c) $|S_{21}|$ of the FSS with optimal sizes fine-tuned by full-wave simulations.

considered in the proposed ECM. As a result, since the mutual capacitances between the three layers of the FSS are ignored, the present ECM can only predict one transmission null in the stopband, while two distinct nulls appear in the full-wave results. Obviously, it is our future work to solve these coupling problems to further improve the accuracy of the ECM for the design of multilayer FSSs. Although the proposed ECM is not perfect, it is still able to provide good initial design data for the multilayer FSSs in a fast manner.

3.2. A Miniaturized Band-Pass FSS with an Absorbing Band. The second example is to design an FSS with a narrow passband near 4.0 GHz in which the transmission efficiency is more than 90% and the reflection coefficient is less than 10% (i.e., $|S_{21}| \geq -0.46$ dB and $|S_{11}| \leq -10$ dB) and a narrow absorbing band around 10 GHz in which the absorption efficiency is more than 80% near 10.0 GHz (i.e., $|S_{21}| \leq -10$ dB and $|S_{11}| \leq -10$ dB). Figure 8 shows the desired frequency response of the S-parameters, and it is seen that both $|S_{21}|$ and $|S_{11}|$ are required to be lower than −10 dB near 10.0 GHz in order to absorb most energy of the incoming EM wave.

From the four building blocks, the FSS with SL elements is chosen to form the narrow passband around 4 GHz, and the FSS with SL elements loaded with lumped resistors [20] is used to obtain a stopband with absorbing ability near 10 GHz in this design. However, the center frequency of the passband is much lower than that of the absorbing band, which makes the sizes of the SS element appreciably larger than those of the SL element. Therefore, in order to arrange the multilayer FSS elements as dense as possible to achieve stable performance of the FSS over a wide range of angles and polarizations of incidence, it is vital to reduce the physical dimensions of the SS element to the similar level of those of the SL element. As shown in Figure 9(a), four capacitors are loaded in the center of each slot to realize the miniaturization. Figure 9(b) shows the EC of the FSS, in which R is the resistor loaded in the SL, while C is the capacitor loaded in the SS. Then, the surface impedances of the two FSS layers are

$$\begin{aligned} Z_1 &= Z_{\mathrm{sl}}^{\kappa} + R, \\ Z_2 &= Z_{\mathrm{ss}}^{\kappa} \parallel \frac{1}{j\omega C}, \end{aligned} \tag{29}$$

where the computation of Z_{sl}^{κ} follows equations (16) and (17) and Z_{ss}^{κ} follows equations (12) and (15). Referring to equations (7)–(10), the circuit parameters L_1, C_1, L_2, and C_2 shown in Figure 9(b) are related to the geometrical sizes from equations (26) and (27):

$$\begin{aligned} L_1 &= \mu_0 \frac{l_{\mathrm{loop}}}{2\pi} \ln\left(\frac{1}{\sin\left(\pi w_{\mathrm{loop}}/2D\right)}\right), \\ C_1 &= \varepsilon_0 \varepsilon_{\mathrm{eff}} \frac{2l_{\mathrm{loop}}}{\pi} \ln\left[\frac{1}{\sin\left(\pi\left(D - l_{\mathrm{loop}}\right)/2D\right)}\right], \\ L_2 &= \mu_0 \frac{l_{\mathrm{slot}}}{2\pi} \ln\left[\frac{1}{\sin\left(\pi\left(D - l_{\mathrm{slot}}\right)/2D\right)}\right], \\ C_2 &= \varepsilon_0 \varepsilon_{\mathrm{eff}} \frac{2\left(l_{\mathrm{loop}} - 2w_{\mathrm{loop}}\right)}{\pi} \ln\left(\frac{1}{\sin\left(\pi w_{\mathrm{loop}}/2D\right)}\right). \end{aligned} \tag{30}$$

Similar to the former design example, if the dielectric substrate is given, the geometrical and EC parameters l_{loop}, l_{slot}, D, R, and C can be obtained by applying the curve-fitting

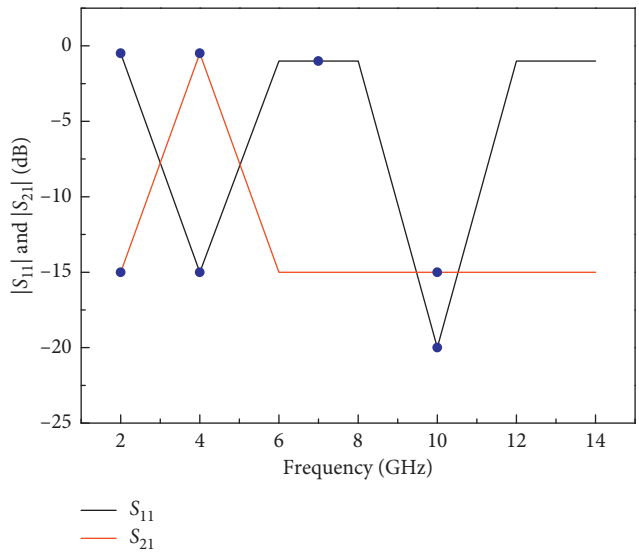

Figure 8: The desired frequency response of $|S_{11}|$ and $|S_{21}|$. The samples marked in blue color are chosen to show the main properties of the FSS in the passband and absorption band.

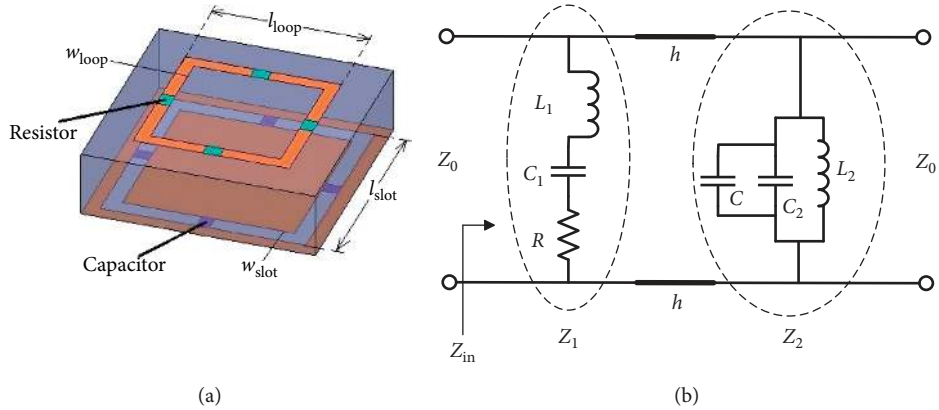

Figure 9: The configuration and equivalent circuit of the miniaturized band-pass FSS with out-of-band absorption. (a) Geometry of one element of the FSS. (b) Equivalent circuit.

method [19] on the samplings from the desired $|S_{11}|$ and $|S_{21}|$ curves in the least-square sense for different angles and polarizations of incidence.

The relative permittivity, loss tangent, and thickness of the dielectric substrate used in this design are 2.2, 0.001, and 2.54 mm, respectively. The width of the SL element w_{loop} is fixed to 0.50 mm, which is the same as the width of the chip resistor, while the width of the SS element w_{slot} is set to 0.64 mm, which is the same as the length of the chip capacitor. The sampling points on the $|S_{11}|$ and $|S_{21}|$ curves are marked in blue color in Figure 8 with quite flexible numbers and positions, if significant performance of the FSS at the sampling frequencies is fully manifested. As an illustration, three and four samples are extracted from the $|S_{21}|$ and $|S_{11}|$ curves, respectively, whose values at the corresponding frequencies are listed in Table 3. Two different angles of incidence ($\theta = 0^\circ$ and 45°) with TE/TM polarization are used to synthesize the parameters l_{loop}, l_{slot}, D, R, and C, and the average values are computed as the design data of the ECM.

Table 3: Samples from the desired frequency response of S_{21} and S_{11}.

Frequency (GHz)	2.0	4.0	7.0	10.0
$\|S_{11}\|$ (dB)	−0.5	−15.0	−1.0	−20.0
$\|S_{21}\|$ (dB)	−15.0	−0.5		−15.0

As in the former example, the ECM data are utilized as the initials of the parameter-sweep process in the full-wave simulator. The final optimal values by the HFSS are $l_{loop} = 6.0$ mm, $l_{slot} = 7.9$ mm, $C = 0.5$ pF, $R = 70.0\,\Omega$, which are very close to the average sizes computed by the proposed ECM. All the parameters obtained in each step during the design process are listed in Table 4.

In Figure 10, the transmission and reflection coefficients of the FSS with the average values of the design parameters by the ECM are shown. The results from the ECM are compared with the numerical results of the HFSS and the desired responses,

Table 4: Equivalent circuit and geometrical parameters calculated by the curve-fitting method.

θ	R (Ω)	C (pF)	l_{loop} (mm)	l_{slot} (mm)	D (mm)
0°	95.01	0.48	6.3	7.9	8.9
45° TE	75.00	0.50	6.7	8.3	9.7
45° TM	73.82	0.54	6.3	7.6	8.5
Averaged values	81.28	0.51	6.4	7.9	9.0
Values after HFSS optimization	70.00	0.50	6.0	7.9	9.0

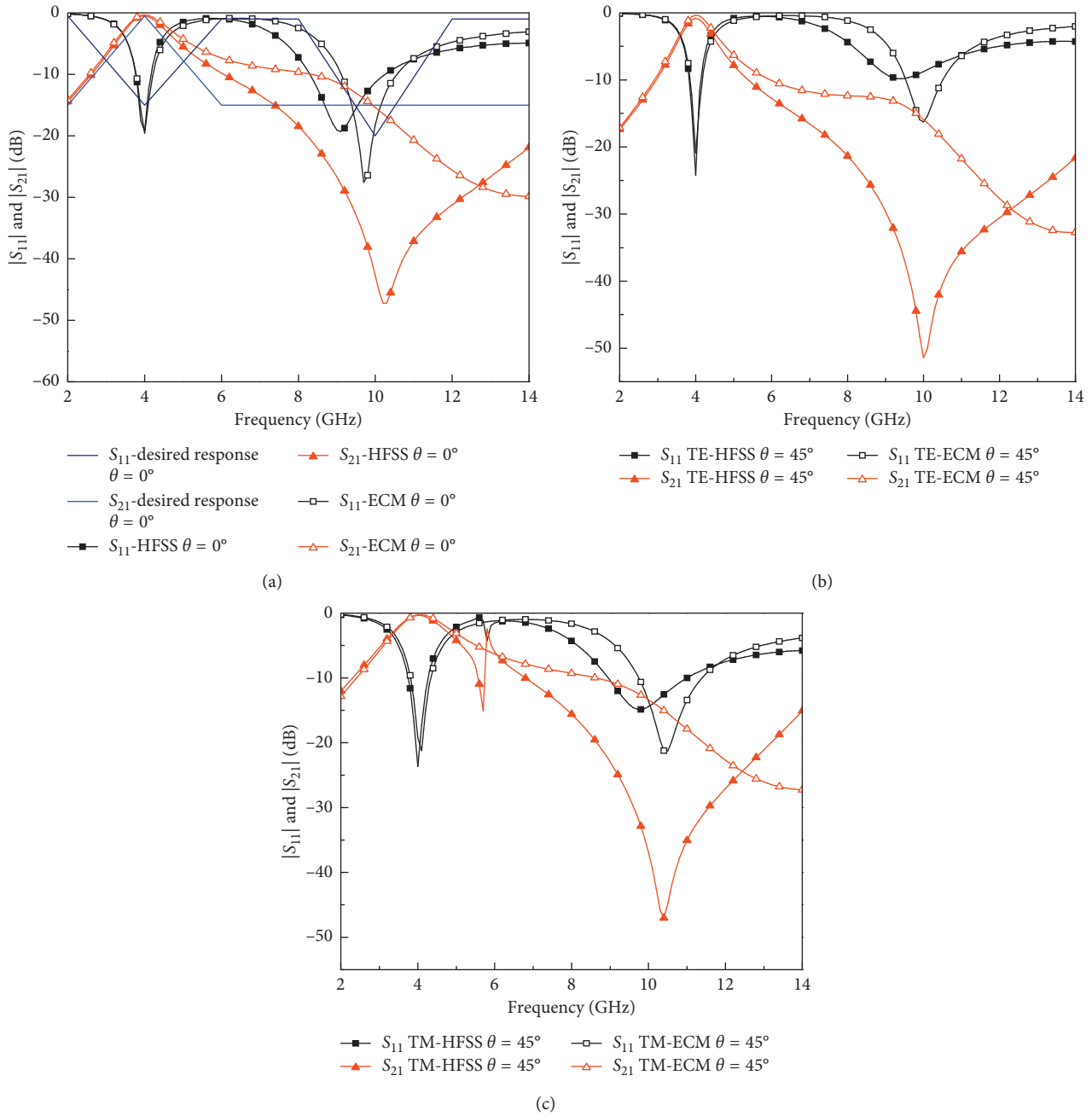

Figure 10: Simulated $|S_{11}|$ and $|S_{21}|$ using the ECM and HFSS. (a) Normal incidence. (b) Oblique incidence at $\theta = 45°$ for TE polarization. (c) Oblique incidence at $\theta = 45°$ for TM polarization.

and it is found that performance of the FSS is stable in the passband and absorbing band for different angles and polarizations of incidence. Figure 11 shows simulated $|S_{11}|$ and $|S_{21}|$ of the optimized FSS structure presented under normal incidence and oblique incidence, when the geometrical sizes and the values of the lumped loads are fine-tuned by the parameter

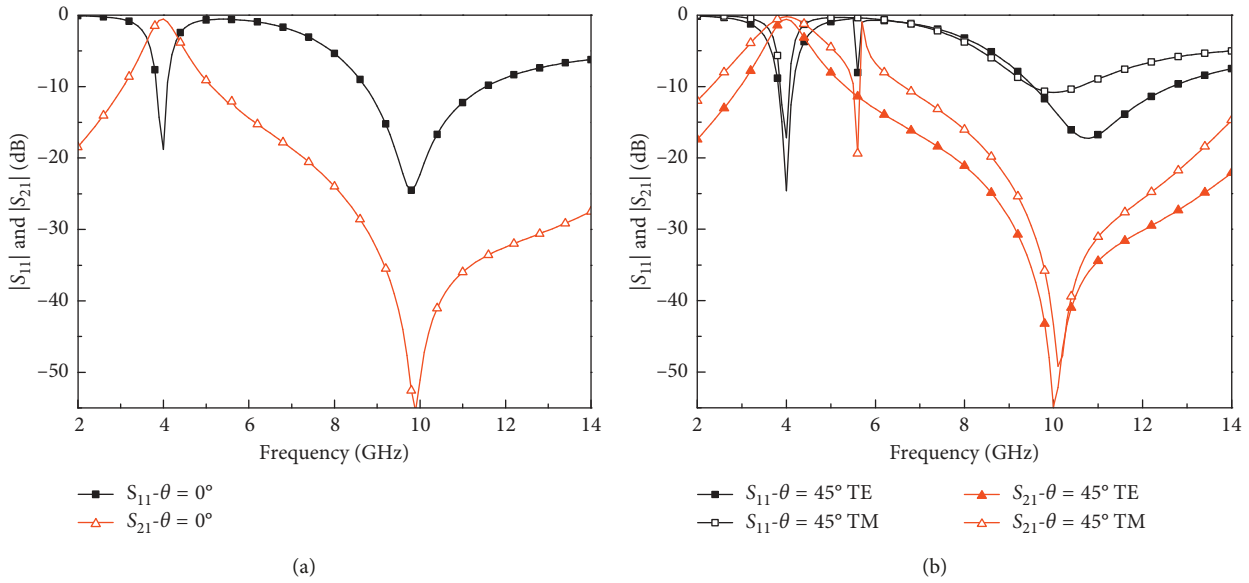

FIGURE 11: Simulated $|S_{11}|$ and $|S_{21}|$ of the FSS with optimal parameters fine-tuned by HFSS simulations. (a) Normal incidence. (b) Oblique incidence at $\theta = 45^{\circ}$ for TE/TM polarization.

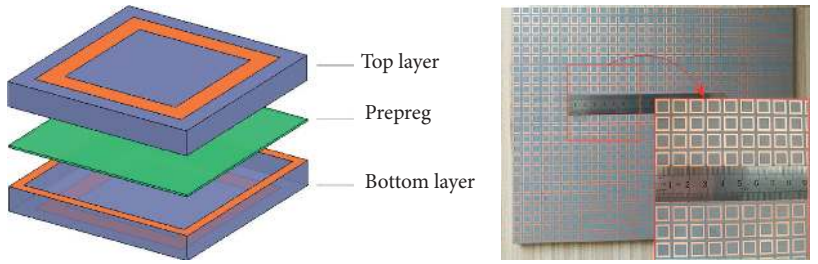

FIGURE 12: Configuration of the band-pass FSS with steep falling edge. (a) Exploded view of the FSS. (b) Photograph of the fabricated prototype.

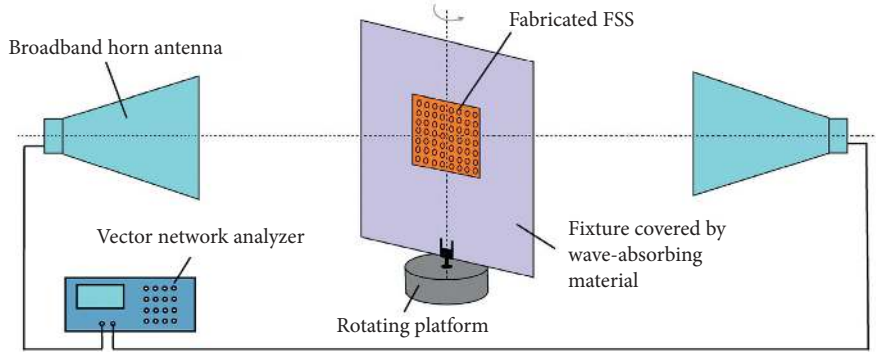

FIGURE 13: Schematic of the measurement setup.

sweep of the HFSS. It is seen that the absorbing efficiency at 10 GHz is improved to 98% when $\theta = 0^{\circ}$ and to 75% or so for both TE and TM polarizations when $\theta = 45^{\circ}$.

4. Experimental Verification

In order to verify the effectiveness of the proposed ECM, the prototype of the first design example, i.e., a multilayer band-pass FSS with a fast falling edge, is fabricated. Figures 12(a) and 12(b) show the configuration and photograph of the fabricated FSS, respectively. The first FSS layer of SL elements is etched on the top of the upper dielectric substrate, and the second SG and third SL FSS layers are etched on the top and bottom of the lower substrate, respectively. Both of the two substrates are Arlon DiClad 880 with $\varepsilon_r = 2.2$ and thickness of 1.27 mm, which are bonded

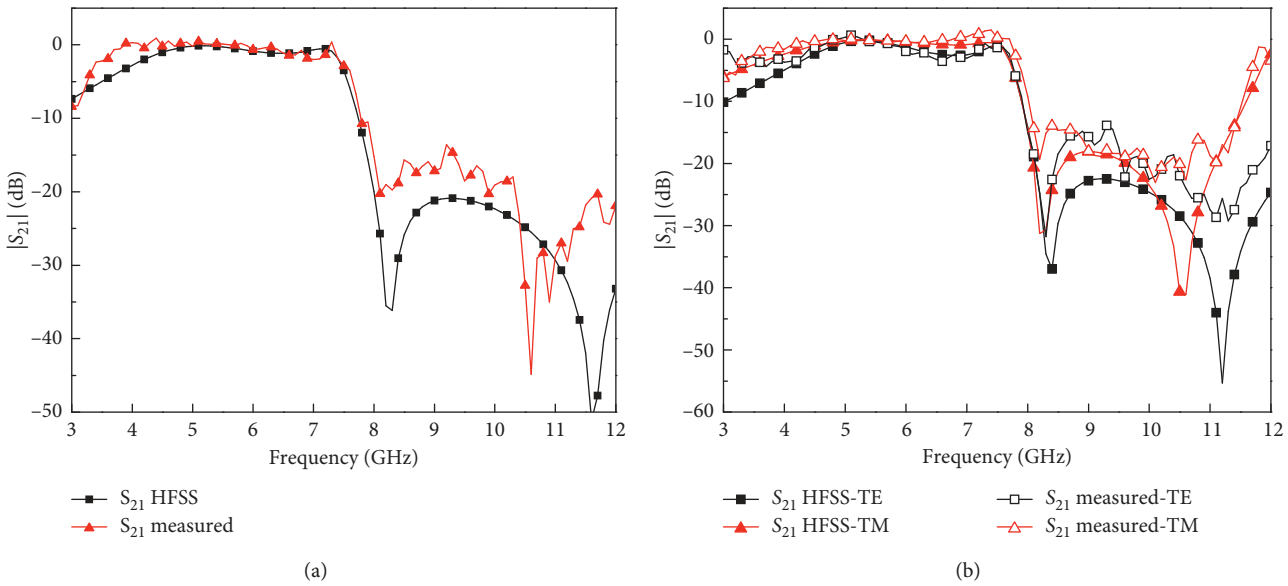

FIGURE 14: Comparison of the measured and the simulated results. (a) $|S_{21}|$ for normal incidence. (b) $|S_{21}|$ for oblique TE/TM incidence of $\theta = 45^{\circ}$.

together by an FR28 prepreg layer with $\varepsilon_r = 2.8$ and thickness of 0.091 mm. The geometrical dimensions of the FSS follow the fine-tuned optimal values in Table 2, i.e., $D = 10.0$ mm, $l_{loop} = 8.2$ mm, $w_{loop} = 1.0$ mm, and $w_{grid} = 1.0$ mm. The lateral size of the prototype is 30.0×30.0 cm^2, which means the number of FSS elements is 30×30.

The measurement setup is shown in Figure 13. It consists of two broadband horn antennas, and a fixture with its four edges being covered by wave-absorbing material is placed between them. The FSS under test is embedded into the fixture, and the line connecting the phase centers of the horn antennas passes through the center of the fixture. The two antennas separate 2.0 m apart to ensure a uniform plane wave impinging upon the FSS. During the measurement of the transmission coefficient of the FSS, we first need to measure $|S_{21}|$ between the horn antennas without the FSS as the calibration data, and then we measure again $|S_{21}|$ between the two horns when the FSS under test is present. Finally, $|S_{21}|$ of the FSS itself is obtained by normalizing $|S_{21}|$ measured in the second time to the calibration data.

Figure 14 shows the measured and numerical results of the $|S_{21}|$ when the angle and polarization of incidence vary. The measured results agree well with the simulated ones, indicating a passband from 4.5 to 7.0 GHz with $|S_{21}| \geq -1.5$ dB, a steep falling edge from 7.0 to 8.0 GHz, and $|S_{21}| \leq -20$ dB through the stopband from 8.0 to 11.0 GHz. In addition, the FSS works stably when the angle of incidence increases up to 45°. At the same time, it is found in Figure 14 that the measured frequency responses have small ripples over the frequency range, which may be caused by multiple reflections between the transmit and receive antennas. Nevertheless, the fabricated prototype meets the desired requirements quite well, which indicates that the proposed design procedure by the four basic building blocks and the ECM is feasible and effective for the multilayer FSSs.

5. Conclusion

A fast design method for the multilayer FSS based on four types of basic building blocks and the equivalent circuit representation is proposed in this paper. The method utilizes the four basic FSS structures to construct multilayer FSSs with desired frequency response of general forms, and the geometrical sizes of the FSS can be synthesized in a fast manner using the ECM. In order to derive equivalent circuit representations of the basic FSSs with adequate accuracy, a complete set of formulas for computation of the surface impedances of the four basic structures is given. The synthesized physical dimensions by the proposed ECM are very close to the fine-tuned values via numerical parameter sweeping process, which indicates that the design method can yield good initials to the full-wave simulators for further optimization. The effectiveness and accuracy of the presented method are verified by numerical and experimental examples.

Data Availability

The data used to support the findings of this study are included within the article.

Conflicts of Interest

The authors declare that there are no conflicts of interest regarding the publication of this paper.

Acknowledgments

The research and publication of this article were funded by the National Natural Science Foundation of China under grant 61471040.

References

[1] B. A. Munk, *Frequency Selective Surface: Theory and Design*, Wiley, New York, NY, USA, 2000.

[2] S. Chakravarty, R. Mittra, and N. R. Williams, "On the application of the microgenetic algorithm to the design of broad-band microwave absorbers comprising frequency-selective surfaces embedded in multilayered dielectric media," *IEEE Transactions on Microwave Theory and Techniques*, vol. 49, no. 6, pp. 1050–1059, 2001.

[3] X.-J. Sheng, J.-J. Fan, N. Liu, and C.-B. Zhang, "A miniaturized dual-band FSS with controllable frequency resonances," *IEEE Microwave and Wireless Components Letters*, vol. 27, no. 10, pp. 915–917, Oct. 2017.

[4] S. Unaldi, S. Cimen, G. Cakir, and U. E. Ayten, "A novel dual-band ultrathin FSS with closely settled frequency response," *IEEE Antennas and Wireless Propagation Letters*, vol. 16, pp. 1381–1384, 2017.

[5] M. Zahir Joozdani and M. Khalaj Amirhosseini, "Equivalent circuit model for the frequency-selective surface embedded in a layer with constant conductivity," *IEEE Transactions on Antennas and Propagation*, vol. 65, no. 2, pp. 705–712, 2017.

[6] N. Liu, X. Sheng, C. Zhang, J. Fan, and D. Guo, "A design method for synthesizing wideband band-stop FSS via its equivalent circuit model," *IEEE Antennas and Wireless Propagation Letters*, vol. 16, pp. 2721–2725, 2017.

[7] M. Al-Joumayly and N. Behdad, "A new technique for design of low-profile, second-order, bandpass frequency selective surfaces," *IEEE Transactions on Antennas and Propagation*, vol. 57, no. 2, pp. 452–459, 2009.

[8] H. Li, Q. Cao, C. Yang, and Y. Wang, "Design and analysis of a frequency selective radome (FSR) with wideband absorbing properties," in *Proceedings of the 2016 IEEE International Workshop on Electromagnetics: Applications and Student Innovation Competition (iWEM)*, pp. 1–3, Nanjing, China, May 2016.

[9] D. Wang, Y.-L. Chow, W. Che, Y. Chang, and K.-S. Chin, "Combined-element frequency selective surfaces with multiple transmission poles and zeros," *IET Microwaves, Antennas & Propagation*, vol. 8, no. 3, pp. 186–193, 2014, https://search.crossref.org/?q=Combined-element+frequency+selective+surfaces+with+multiple+transmission+poles+and+zeros.

[10] S. A. Tretyakov, *Analytical Modeling in Applied Electromagnetics*, Artech House, Norwood, MA, USA, 2003.

[11] O. Luukkonen, "Artificial impedance surfaces," Ph.D. Dissertation, Department of Radio Science and Engineering, Helsinki University of Technology, Espoo, Finland, 2009.

[12] N. Marcuvitz, *Waveguide Handbook*, McGraw-Hill, New York, NY, USA, 1951.

[13] O. Luukkonen, C. Simovski, G. Granet et al., "Simple and accurate analytical model of planar grids and high-impedance surfaces comprising metal strips or patches," *IEEE Transactions on Antennas and Propagation*, vol. 56, no. 6, pp. 1624–1632, 2008.

[14] R. J. Langley and E. A. Parker, "Equivalent circuit model for arrays of square loops," *Electronics Letters*, vol. 18, no. 7, pp. 294–296, 1982.

[15] C. K. Lee and R. J. Langley, "Equivalent-circuit models for frequency-selective surfaces at oblique angles of incidence," *IEE Proceedings H Microwaves, Antennas and Propagation*, vol. 132, no. 6, pp. 395–399, 1985.

[16] G. Sung, K. Sowerby, M. Neve, and A. Williamson, "A frequency-selective wall for interference reduction in wireless indoor environments," *IEEE Antennas and Propagation Magazine*, vol. 48, no. 5, pp. 29–37, 2006.

[17] D. Ferreira, R. F. S. Caldeirinha, I. Cuinas, and T. R. Fernandes, "Square loop and slot frequency selective surfaces study for equivalent circuit model optimization," *IEEE Transactions on Antennas and Propagation*, vol. 63, no. 9, pp. 3947–3955, 2015.

[18] ANSYS HFSS, *ANSYS Design Modeler. Design Exploration User's Guide ANSYS Workbench*, ANSYS HFSS, Canonsburg, PA, USA, 2013, https://www.ansys.com.

[19] N. Kou, Y. Shi, and L. Li, "Dual-pass band equivalent circuit analysis for frequency selective surfaces," in *Proceedings of the 2015 IEEE International Conference on Communication Problem-Solving (ICCP)*, pp. 402–404, Guilin, China, October 2015.

[20] S. Ghosh and K. V. Srivastava, "An equivalent circuit model of FSS-based metamaterial absorber using coupled line theory," *IEEE Antennas and Wireless Propagation Letters*, vol. 14, pp. 511–514, 2015.